

Experimental Development of Solar Collector of Unconventional Air

J. O. Almirón, M. A. Lara *

Alternative Energy Laboratory (FCEIA-IFIR-UNR-CONICET), Av. Pellegrini 250 - CP 2000 – Rosario, Argentina

*Corresponding author: malara@fceia.unr.edu.ar

Abstract Is designed and built a solar air collector, corresponding to an elliptical collector format, in order to analyze their energy performance in terms of thermal efficiency and feasibility, to be used in agro-industrial processes and environments conditioning habitat. Experimental data were surveyed to quantify and substantiate efficiency of the device as a heat exchanger. These results were favorable than expected before construction. Average values less than 25% efficiency were expected, and average values of 28.7% were obtained. The velocity values of internal air tested were between 1.1 and 1.83 m/seg., and angles experienced were 44 ° and 40° to the horizontal plane. The final conclusion allows us to demonstrate that the unconventional system can obtain the same results as conventional air collectors in terms of operability and heat exchange.

Keywords: solar energy, collector, heat transfer, efficiency

Cite This Article: J. O. Almirón, and M. A. Lara, “Experimental Development of Solar Collector of Unconventional Air.” *Sustainable Energy*, vol. 4, no. 1 (2016): 17-27. doi: 10.12691/rse-4-1-3.

1. Introduction

The physical principle governing the transfer of heat inside the solar collectors with transparent cover, is the greenhouse effect, which occurs when solar radiation passes through the transparent cover of the collector (shortwave radiation), and it is trapped inside the same. The cover is opaque to longwave radiation, which it corresponds to emissions energy as heat (infrared spectrum). When most of the solar radiation through the cover, a portion is reflected by the absorber plate, returning radiation to impinge on the inner side of the cover, where it is driven back to the absorber plate. In this way, the fluid flowing on the inside, absorbs the heat energy of the plate. For this case, the fluid is air.

The density, heat capacity and thermal conductivity of air are low, limiting the thermal efficiency of solar collectors. These devices are used for small increments air temperature. Then, it is desirable to optimize heat transfer between absorber plate and air through turbulent flow, helped by a fan or increasing the transfer area.

There are also these devices with double transparent cover on the absorber plate, which improves performance heat extraction, and is appropriate to use when the air temperature increases are greater than 30, regarding ambient temperature. A increases lower air temperature, it should work with collectors single cover, because collectors double deck have reflection losses in the second window, behaving less efficient than a cover [1,2].

The Solar air collectors planes, currently are design under rectangular or square geometries, for its easy operation and satisfactory results in reference to thermal efficiencies and structural conditions as stiffness and tightness; also mathematical models are well defined [3],

which fit the physical reality with remarkable concordance. With the new elliptical geometry, it seeks to achieve that the proposed model fits reality with good accuracy.

The experiment was conducted in the city of Rosario, Province of Santa Fe - Argentina. The collected data correspond to measurements of temperature inside at the ends and in the center of the collector, both above and below the absorber plate; Irradiance measurement site, measurement speed of entry and exit of air. The dates correspond to experimental day 14/07/2012, 20/07/2012, 25/08/2012, 26/08/2012, 02/09/2012, 08/09/2012, 09/09/2012 and 13/10/2012; in the interval time from 11 hours to 15 hours. The time in question is local time.

2. Description of the Prototype

The constructed system is composed of a solar collector elliptical, where the ellipse is formed by two covers, one of cellular polycarbonate of 4 mm thick and 5.8 m x 1.03 m. The other plate glass fiber is 800 g/m², thickness of 3 mm, and 1.03 x 5.8 m. There is an absorber plate inside made of galvanized sheet 1.25 mm of thickness and 1 m x 5.8 m, and painted matte black [4]. This plate divides the interior compartment into two parts circulation; the upper and lower. The lower plate of polycarbonate is thermally insulated with polyurethane foam 10 mm of thickness.

The upper plate of polycarbonate alveolar, is curved in the direction of the alveoli and a maximum sagitta of 14 cm. A lower plate has a maximum sagitta of 15 cm. Given the dimensions of the plate it was necessary to attach plates cut to size, using scotch tape, given that the union H polycarbonate plates were broken by bending.

The extremes of the laterls unions of the absorber plate, are made with aluminum profiles, where the inside is isolated with rubber and profiles cling to this by screws.

The system orientation is north, being located horizontally from east to west. With this location is not considered greatly affected the optical properties of the collector, either morning or afternoon by the effect of the ribs of polycarbonate [5]. To ensure turbulence in the collector [6], there are every meter of absorbent baffles both above and below, made of galvanized strips and painted matte black. The support structure is made with square sections of iron of 50 mm x 30 mm x 1000 mm, soldiers in L and painted black.

In the extreme horizontal of the supports, there are hinges iron black in color, welded on one side, allowing free movement of the other half. The hinges have 140 mm long each sheet.

In the extreme vertical of the supports there iron hinges, which allows adjusting the angle of the collector, displacing the hinges through bolts screwed to the support. Also, there are structures U-shaped iron, bolted between these hinges and collector, with the purpose of comply with the desired angle.

Once armed the solar collector, the two elliptical mouths are coupled at the extremes thereof. One of them is to regulate the air flow circulated (damper), the other mouth is to ligate the collector with polyethylene the fan. This union is made with transparent polyethylene 200 microns. Transparency assures that does not interfere measurement of temperature in the inlet collector. This plastic is sealed laterally to give hermeticism to the enclosure.

3. Collector Test

Device for testing, thermocouples are placed in the absorber plate above and below this, in the central part and at the extremes, having six temperature measuring points; 2 thermocouples are placed in polyethylene foam insulation in the inlet and outlet collector; 1 on polycarbonate plate. Is used for this, a data acquisition CR 23 X Micrologger, brand Campbell Scientific, Inc.

To determine the air temperature, are placed 6 electronic temperature recorders, brand Novus on the input, output and central collector are placed above and below the absorber plate. These data loggers are scheduled to begin acquiring data through memory, to be later sent to an order and to display the data. The use of LogChart-II software is the tool used for configuration.

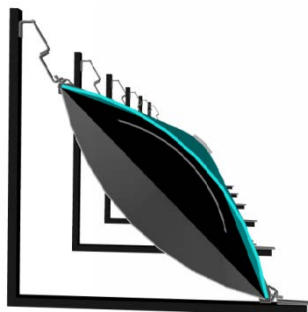
In total there are 9 thermocouples to sense temperature materials, and 6 to sense internal air temperature. Simultaneously, radiation measurements in situ for the inclination of the collector were counted.

External air temperature and humidity thereof are also measured by electronic recorder Novus, which contains two input channels for two simultaneous measurements. The principle of operation is similar to electronic temperature recorder.

To measure flow velocities, is available 1 anemometer brand Wilh Lambrecht Göttingen. To vary the flow velocity, is connected to the fan, a transformer brand Variostat, to vary the speed by varying the output voltage.



Photo 1. Photo of the experimental prototype

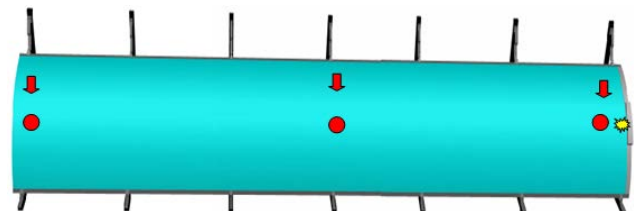


Scheme 1. Front view the east of the collector

In scheme 1, red arrows indicate the location of thermocouples, both above and below the plate. The same goes with red circles indicating the positions of the electronic temperature recorders.

In scheme 2, the irregular circle yellow is solarimeter position. Red arrows and red circles indicating the

position of recorders and thermocouples located from another view.



Scheme 2. Front view of the solar collector

4. Considerations Thermal Collector

When enter a fluid at a uniform speed in geometry as rectangular and circular sections, and when this fluid comes into contact with the surface under conditions of laminar regime, viscous effects are becoming important.

When the fluid particles make contact with a surface gain null speed; these particles retard the movement of fluid layers adjoining to the mainstream, which in turn retards the movement of the particles of the following layers to a certain distance parallel to the fluid stream, where it become insignificant. These delays the movement of the fluid are associated with shear forces which act in planes which are parallel to the fluid velocity.

This distance is called thickness limit layer, being this, the value where the fluid velocity is 99% of the current velocity. In this way, the speed varies with distance, through the limit layer. After the union of the limit layers (above and below this section), viscous effects extend over the entire cross section and the velocity profile does not change with increasing distance of this geometry. It is said that the flow is *fully developed*, and the distance from the entrance until where this condition is reached, it is usually called hydrodynamic limit layer.

For the case of turbulent flow, the velocity profile is flat. The turbulence begins to numbers of Reynolds greater than 2300, although necessary numbers of Reynolds greater (Reynolds ≈ 10000) to achieve fully turbulent conditions. The hydrodynamic limit layer of this regime, even though does not have a satisfactory general expression, it is independent of the number of Reynolds, and the following approximation is considered valid:

$$10 \leq (x / De)_{turbulent} \leq 60. \quad (1)$$

Considering thermal effects; at the beginning of a flat plate, the temperature profile of flow is uniform.

However, the fluid particles that make contact with plate, reach thermal equilibrium at the temperature the surface of the plate, achieved a temperature gradient toward the center of the fluid stream. The region of the fluid that reach this gradient, it called thermal limit layer. Within the duct develops an upper and lower limit layer. In the longitudinal direction there is a thermal region of entrance, until the point where these limit layers are joined.

For the turbulent region, the approach to this regime where the thermal conditions are fully developed is as follows:

$$(x / De)_{turbulent} \approx 10. \quad (2)$$

So, for flow thermally fully developed of a fluid with constant properties, the convection coefficient is independent of the length. Since the thickness of thermal limit layer is zero at the entrance of the plate, the convection coefficient is extremely large in $x=0$. However, this coefficient decreases rapidly as the thermal limit layer develops, until it reaches the constant value.

The equivalent diameter of the oval [7] is:

$$De = 1,55 * (A1^{0,625}) / P^{0,25} \quad (3)$$

$$A1 = \left[(\pi * r^2) / 4 \right] + r * (s - r). \quad (4)$$

For this case, the width of the fixed plate is of 1 m, but it has been taken as a string s , equivalent to 0,45 m. This is considering that 10% of this plate is not absorbed by shadow generated by aluminum profiles.

The serie of the perimeter formula of the ellipse, takes infinite terms, but for the purposes of the calculation, it is taken until the third term. The mistake for not considering the following summands is negligible. In this case the perimeters of each semi-ellipse are added together (because having different sagittae upper and lower plates). The total perimeter will be:

$$h_i = (r_i - s)^2 / (r_i + s)^2 \quad (5)$$

$$P = \sum P_i = (\pi / 2) * (r_i + s) * \left[\begin{array}{l} 1 + (1/4) * h_i \\ + (1/64) * h_i^2 \\ + (1/256) * h_i^3 + \dots \end{array} \right]. \quad (6)$$

Table 1 shows the geometric measures of the solar air collector.

Table 1. Measures geometric solar air collector

| Collector Seccion | r (m) | s (m) | A1 (m) | P (m) | De (m) | x/De |
|-------------------|-------|-------|--------|-------|--------|------|
| Upper | 0,14 | 0,45 | 0,0294 | 0,992 | 0,171 | 33,9 |
| Lower | 0,15 | 0,45 | 0,0313 | 1,002 | 0,178 | 32,6 |

The minimum length upper for flow developed will be according to equation (1) equal to 1,71 m.

The minimum length lower for flow developed will be according to equation (1) equal to 1,78 m.

So, is set the approach to turbulent flow of flow fully developed is met, because the previous relationship, is greater than the minimum length for the flow to be fully developed.

Table 2. Emissivity (ξ_p), absorbance (α_p) and reflectance (ρ_p) of the absorber plate. Emissivity (ξ_c), transmittance (ζ_c) and reflectance (ρ_c) of the polycarbonate plate 4 mm of thickness

| Collector Inclination ($^\circ$) | ξ_p | α_p | ρ_p | ξ_c | ζ_c | ρ_c |
|------------------------------------|---------|------------|----------|---------|-----------|----------|
| 40 | 0,96 | 0,96 | 0,04 | 0,746 | 0,746 | 0,05 |
| 44 | 0,96 | 0,96 | 0,04 | 0,746 | 0,746 | 0,05 |

6. Efficiency Solar Collector

The solar collectors are tested, following the standard procedure recommended by National Boreal of Standard

5. Optical Characteristics of Materials Used

The materials used were: absorber plate painted matte black and the upper plate of alveolar polycarbonate, whose optical characteristics are:

consisting of operating the collector under stable conditions of solar radiation, wind speed, fluid flow, fluid temperature at the inlet and outlet, ambient temperature, for a period of time where the useful energy not

significantly vary [8]. So the useful energy without considering the fan [3] is:

$$qu = m * Cp * Af * (Tms - Ta) \quad (7)$$

$$m = \rho * v \quad (8)$$

Where Af is equivalent to $0,42 \text{ m} * 0,12 \text{ m} = 0,05 \text{ m}^2$, corresponding to the area of fluid outlet.

The effective efficiency of the collector [9] is performed for each sector, that is, above the absorber plate and below this plate, then the mean efficiency between the two sectors is obtained calculated as:

$$\eta = \frac{(qu - P / 0.18)}{(I * A)} \quad (9)$$

In this way the collector efficiency will be the net thermal gain. That is, increase energy air, should subtract from the frictional thermal energy to move the internal air. The density, calorific capacity and thermal conductivity of air is low, limiting the thermal efficiency of the solar collectors. Then, it is desirable to optimize the heat transfer between absorber plate and air through turbulent flow, aided by fan or increasing the transference area.

The energy performance curve of collector obtained by plotting η vs $\Delta T/I$, where the last expression, is calculated, equaling the useful heat as follows:

$$\begin{aligned} A * [(I * \alpha p * \zeta c - Up * (Tp - Ta))] \\ = Af * Cp * \rho * v * (Tms - Ta) \end{aligned} \quad (10)$$

$$\begin{aligned} \Delta T / I &= (Tp - Ta) / I \\ &= [(\alpha p * \zeta c) / Up] \left\{ \frac{Af * Cp * \rho * v}{v * (Tms - Ta)} \right\} / (I * A * Up). \end{aligned} \quad (11)$$

6.1. Conversion Factor of Mechanical Power in Thermal Energy

This factor arises from taking into account the product of the individual efficiencies of a process, whereas mechanical energy is obtained from a thermal power plant [10].

Summarizing, the efficiency will be the product of the individual efficiencies of the process of generation, transmission and fan energy consumption. For this case, it will be defined in the following manner:

$$\eta_{total} = \eta_{thermal \text{ power plant}} * \eta_{electric \text{ power transmission}} * \eta_{fan \text{ motor}} * \eta_{fan} \quad (12)$$

$\eta_{thermal \text{ power plant}} = 0,344$ (also involved electrical distribution)

$\eta_{electric \text{ power transmission}} = 0,925$

$\eta_{fan \text{ motor}} = 0,88$

$\eta_{fan} = 0,65$

$\eta_{total} = 0,18.$

7. Measurements Made

In Table 3, are tabulated average daily temperatures.

Table 3. Average daily temperatures. Ta, ambient temperature; Tf, upper fluid temperature; Tf1 lower temperature fluid; Tc, upper cover temperature; Tc1, temperature lower cover; Tp temperature above the plate; Tp1 temperature below the plate. The values are the daily averages in the time interval sampled

| TEMP. (°C) | DATE | | | | | | | | |
|---------------|--------|--------|--------|--------|--------|--------|--------|--------|--------|
| | 14/07 | 20/07 | 25/08 | 26/08 | 02/09 | 08/09 | 09/09 | 11/09 | 13/10 |
| Ta | 11,67 | 20,22 | 13,78 | 14,68 | 28,90 | 22,17 | 17,26 | 23,63 | 25,86 |
| Tf | 38,85 | 40,81 | 43,92 | 32,93 | 49,13 | 55,22 | 51,35 | 82,41 | 53,76 |
| Tf1 | 24,99 | 37,46 | 31,15 | 25,71 | 49,34 | 41,55 | 29,96 | 54,64 | 40,76 |
| Tc | 18,99 | 32,30 | 38,75 | 25,48 | 41,81 | 47,39 | 32,76 | 76,02 | 38,88 |
| Tc1 | 17,92 | 31,76 | 29,63 | 24,08 | 40,84 | 38,67 | 29,81 | 41,15 | 37,10 |
| Tp | 56,00 | 53,64 | 63,51 | 48,31 | 67,23 | 66,97 | 63,01 | 82,00 | 69,97 |
| Tp1 | *36,90 | *44,29 | *48,41 | *36,80 | *54,28 | *57,62 | *46,66 | *67,94 | *56,79 |

* These values temperatures are not considered for the calculations, due to their difference with the upper temperature of the absorber plate (Tp). For subsequent calculations, Tp1 equals Tp.

Whereas that the thermal conductivity of the absorber plate is $50 \text{ W/m} \cdot \text{°C}$, then the thermal resistance of the heat conduction plate (L/k) is equal to $2,5 \times 10^{-5} (\text{W} / \text{°C})^{-1}$.

This value is very small, and a heat flow well above available is needed from the expected maximum solar

radiation, so that there is a considerable thermal gradient in the plate.

Also, tabulated the average daily radiation incident during the experience, according to Table 4.

Table 4. Average daily radiation in the time interval sampled, that reaches the polycarbonate

| | DATE | | | | | | | | |
|-------------|-------|-------|-------|-------|-------|-------|-------|-------|-------|
| | 14/07 | 20/07 | 25/08 | 26/08 | 02/09 | 08/09 | 09/09 | 11/09 | 13/10 |
| Rad.(kW/m2) | 0,92 | 0,75 | 1,01 | 0,74 | 0,86 | 0,97 | 0,98 | 0,87 | 1,04 |

Meteorological data, together with internal air speed and incline of the collector, for each date and time are shown in Table 5.

Table 5. Information collected on experience, in terms of hours, voltage, fan, internal fluid velocity, angle of the collector, as well as the weather

| Date | Time | Voltaje (Volt) | Speed (m/seg.) | Inclination (°) | Climate |
|------------|-------|----------------|----------------|-----------------|----------------------|
| 14/07/2012 | 11 | 150 | 1.25 | 40 | Totally Clear Sky |
| | 12 | 225 | 1.80 | 40 | |
| | 13 | 150 | 1.25 | 44 | |
| | 14 | 225 | 1.80 | 44 | |
| 20/07/2012 | 12:00 | 150 | 1.15 | 40 | Clear Sky |
| | 12:30 | 225 | 1.5 | 44 | |
| | 13 | 150 | 1.58 | 44 | |
| 25/08/2012 | 11:55 | 150 | 1,35 | 40 | Clear Sky |
| | 12:30 | 225 | 1,5 | 40 | |
| | 13 | 150 | 1,15 | 44 | |
| | 14 | 225 | 1,58 | 44 | |
| 26/08/2012 | 11 | 150 | 1,4 | 44 | Partially Cloudy Sky |
| | 12 | 225 | 1,63 | 44 | |
| | 13 | 150 | 1,5 | 40 | |
| | 14 | 225 | 1,83 | 40 | |
| 02/09/2012 | 11 | 150 | 1,4 | 40 | Totally Clear Sky |
| | 12 | 225 | 1,75 | 40 | |
| | 13 | 150 | 1,3 | 44 | |
| | 14 | 225 | 1,7 | 44 | |
| 08/09/2012 | 13:30 | 150 | 1,43 | 44 | Totally Clear Sky |
| | 14 | 225 | 1,3 | 44 | |
| 09/09/2012 | 11 | 150 | 1,35 | 40 | Clear Sky |
| | 12 | 225 | 1,5 | 40 | |
| | 13 | 150 | 1,15 | 44 | |
| | 14 | 225 | 1,58 | 44 | |
| 11/09/2012 | 11 | 0 | 0 | 40 | Partially Cloudy Sky |
| | 12 | 0 | 0 | 40 | |
| | 13 | 0 | 0 | 40 | |
| | 14 | 0 | 0 | 40 | |
| 13/10/2012 | 11 | 150 | 1,1 | 40 | Totally Clear Sky |
| | 12 | 225 | 1,75 | 40 | |
| | 13 | 150 | 1,15 | 44 | |
| | 14 | 225 | 1,7 | 44 | |

8. Graphics Performance Solar Collector

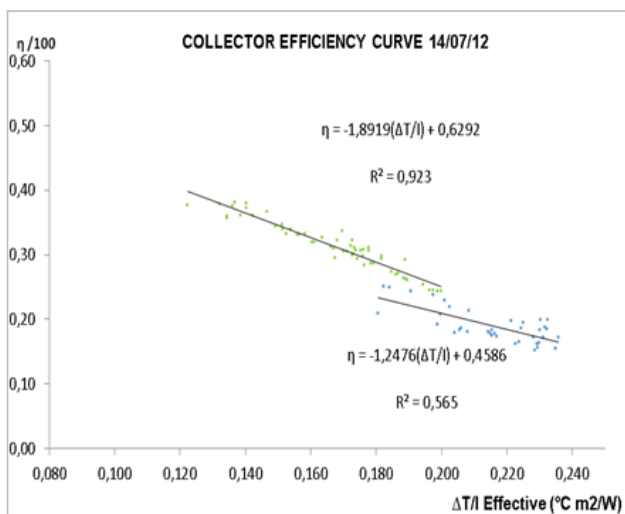


Figure 1. Efficiency collector as a function of $\Delta T/I$ the day 14/07/12, and flow velocity 1.25 m/sec

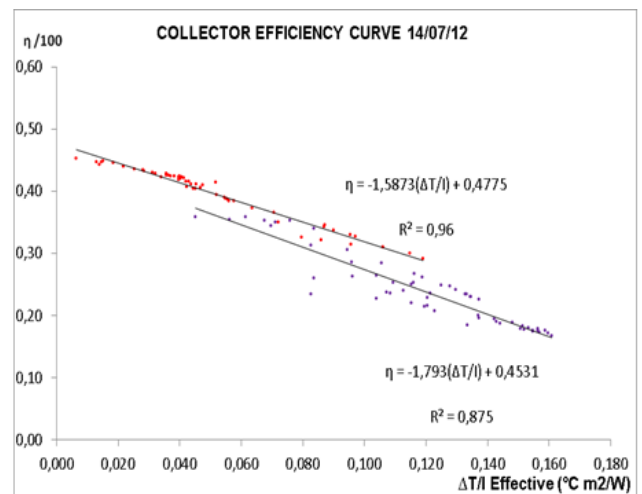


Figure 2. Efficiency collector as a function of $\Delta T/I$ the day 14/07/12, and flow velocity 1.8 m/sec

Blue points: in the schedule from 11:20 hs to 12:00 hs and collector tilt angle 40 °.

Green points in the schedule from 13:00 hs to 14:00 hs and collector tilt angle 44 °.

Red points in the schedule from 12:00 hs to 13:00 hs and collector tilt angle 40 °.
Lilacs points: in the schedule from 14:00 hs to 15:00 hs and collector tilt angle 44 °.

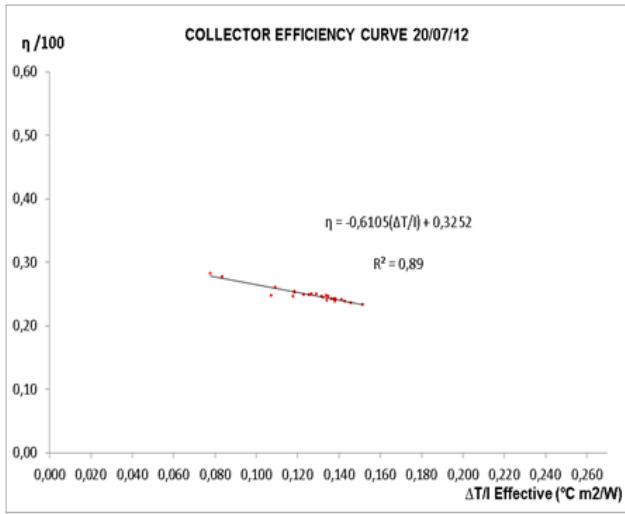


Figure 3. Efficiency collector as a function of $\Delta T/I$ the day 20/07/12, and flow velocity 1.5 m/sec

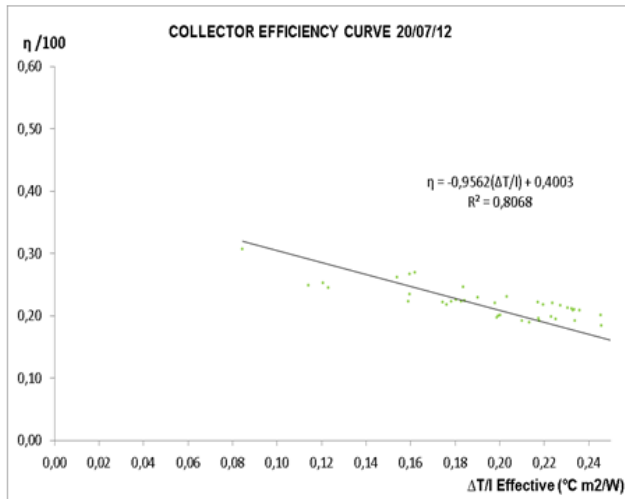


Figure 4. Efficiency collector as a function of $\Delta T/I$ the day 20/07/12, and flow velocity 1.58 m/se

Red points: in the schedule from 12:30 hs to 13:00 hs and collector tilt angle 44 °.
Green points: in the schedule from f 13:00 hs to 14:00 hs and collector tilt angle 44 °.

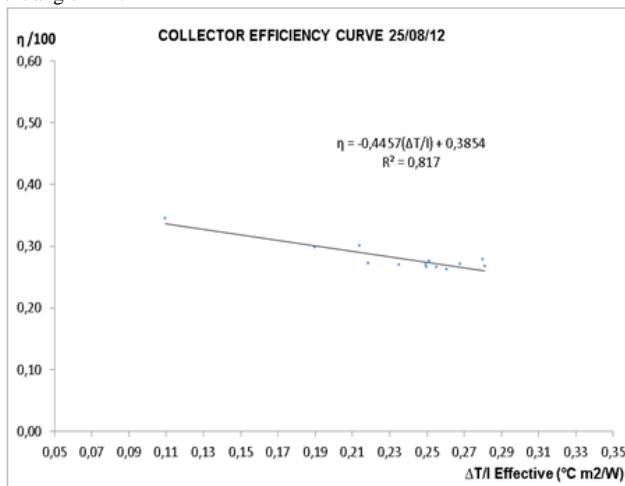


Figure 5. Efficiency collector as a function of $\Delta T/I$ the day 25/08/12, and flow velocity 1.35 m/sec

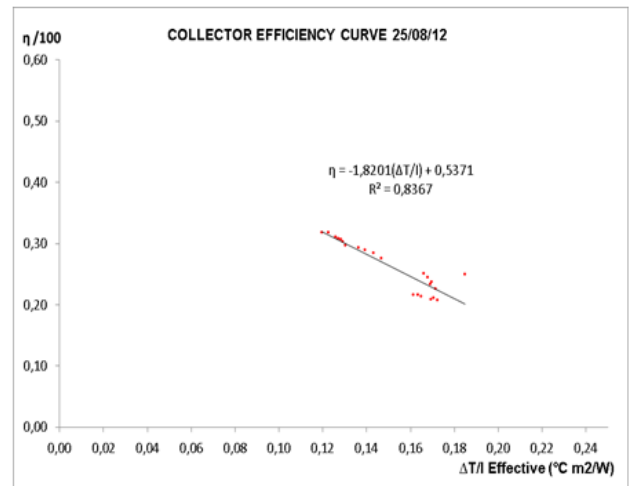


Figure 6. Efficiency collector as a function of $\Delta T/I$ the day 25/08/12, and flow velocity 1.5 m/sec

Blue points in the schedule from 12:00 hs to 12:30 hs and collector tilt angle 40 °.

Red points: in the schedule from 12:30 hs to 13:00 hs and collector tilt angle 40 °.

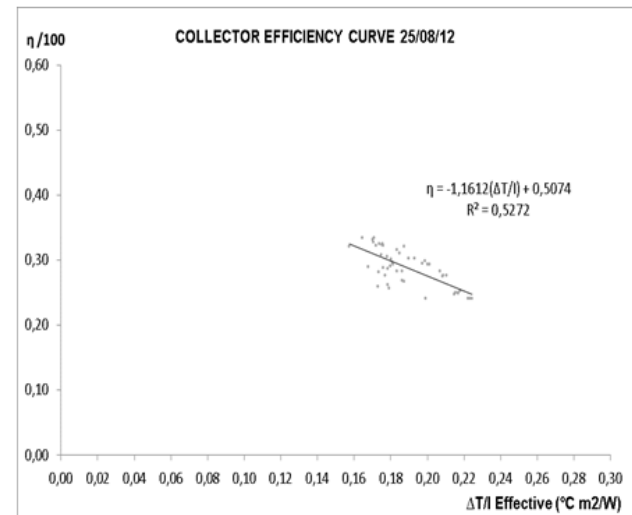


Figure 7. Efficiency collector as a function of $\Delta T/I$ the day 25/08/12, and flow velocity 1.15 m/sec

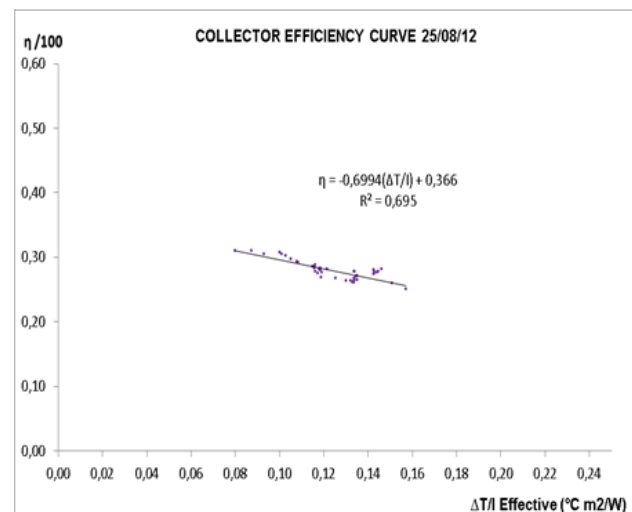


Figure 8. Efficiency collector as a function of $\Delta T/I$ the day 25/08/12, and flow velocity 1.58 m/sec

Green points: in the schedule from 13:00 hs to 14:00 hs and collector tilt angle 44 °.

Lilacs points: in the schedule from 14:00 hs to 15:00 hs and collector tilt angle 44 °.

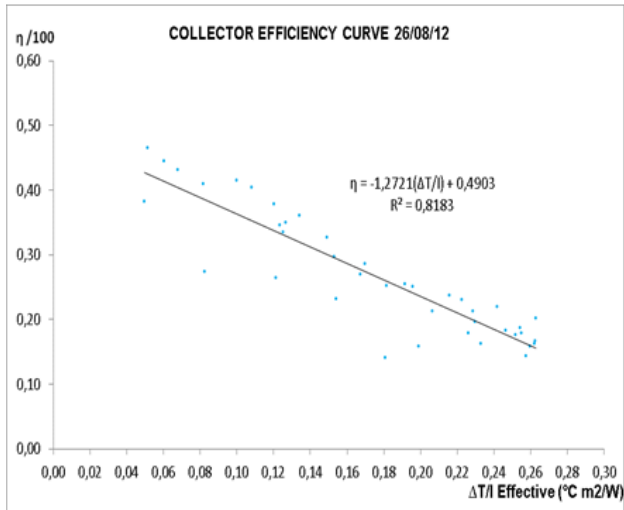


Figure 9. Efficiency collector as a function of $\Delta T/I$ the day 26/08/12, and flow velocity 1.4 m/sec

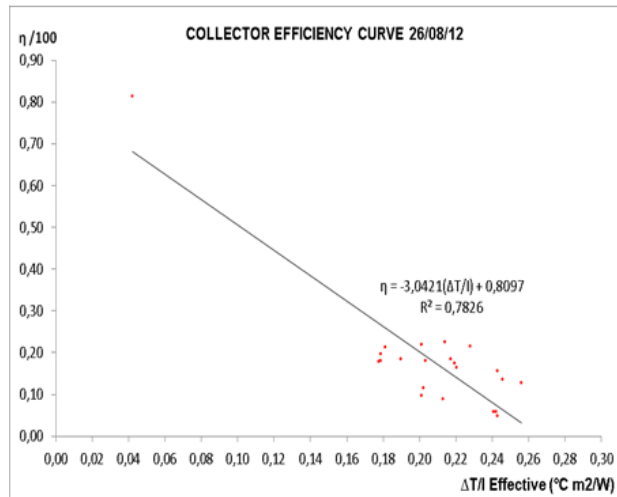


Figure 10. Efficiency collector as a function of $\Delta T/I$ the day 26/08/12, and flow velocity 1.63 m/sec

Sky-blue points: in the schedule from 11:00 hs to 12:00 hs and collector tilt angle 44 °.

Red points: in the schedule from 12:00 hs to 13:00 hs and collector tilt angle 44 °.

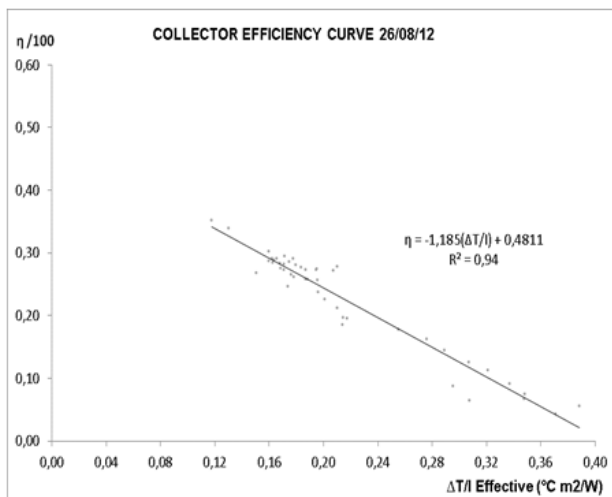


Figure 11. Efficiency collector as a function of $\Delta T/I$ the day 26/08/12, and flow velocity 1.5 m/sec

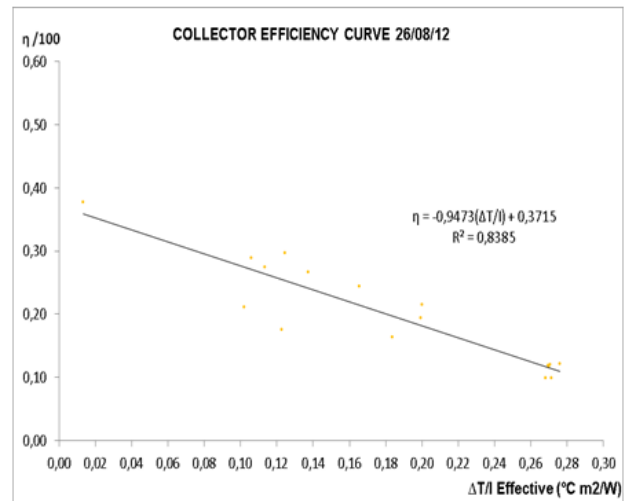


Figure 12. Efficiency collector as a function of $\Delta T/I$ the day 26/08/12, and flow velocity 1.83 m/sec

Green points: in the schedule from 13:00 hs to 14:00 hs and collector tilt angle 40 °.

Yellow points: in the schedule from 14:00 hs to 15:00 hs and collector tilt angle 40 °.

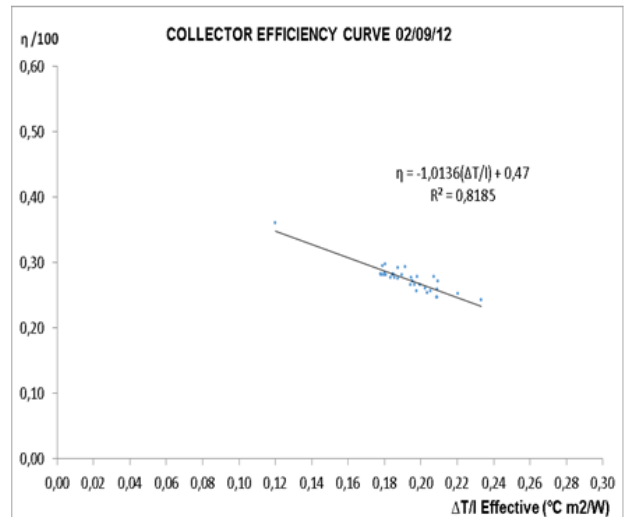


Figure 13. Efficiency collector as a function of $\Delta T/I$ the day 02/09/12, and flow velocity 1.4 m/sec

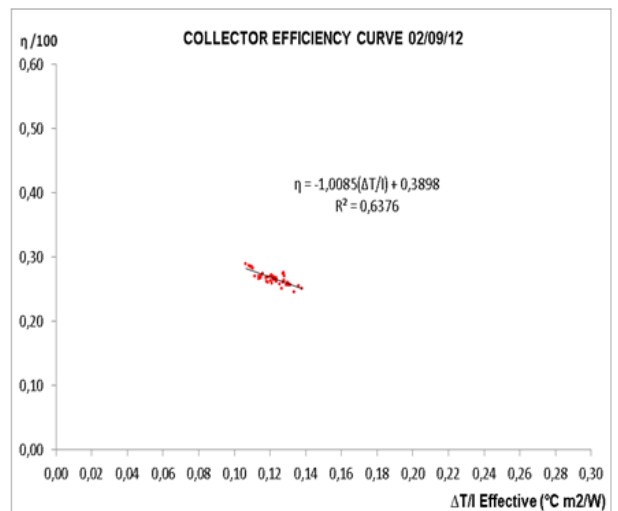


Figure 14. Efficiency collector as a function of $\Delta T/I$ the day 02/09/12, and flow velocity 1.75 m/sec

Blue points: in the schedule from 11:00 hs to 12:00 hs and collector tilt angle 40 °.

Red points: in the schedule from 12:00 hs to 13:00 hs and collector tilt angle 40 °.

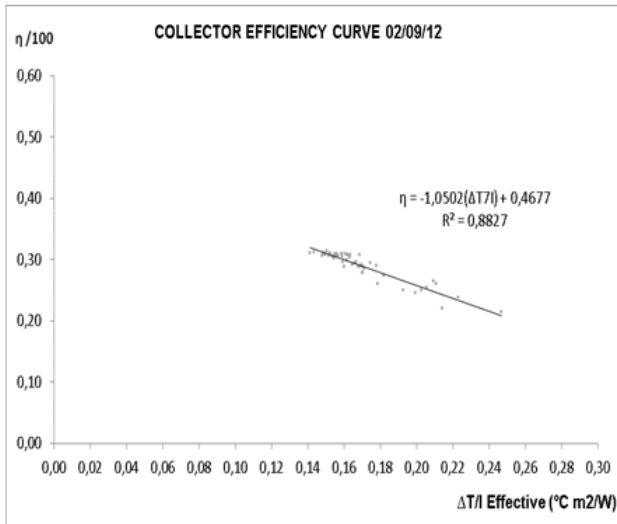


Figure 15. Efficiency collector as a function of ΔT/I the day 02/09/12, and flow velocity 1.3 m/sec

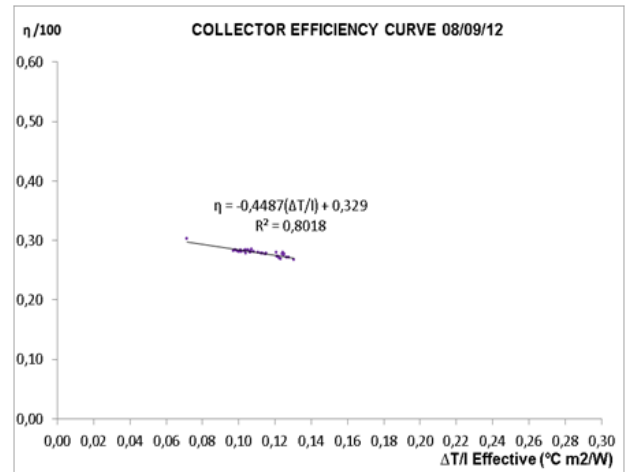


Figure 18. Efficiency collector as a function of ΔT/I the day 08/09/12, and flow velocity 1.3 m/sec

Green points: in the schedule from 13:00 hs to 14:00 hs and collector tilt angle 44 °.

Lilacs points: in the schedule from 14:00 hs to 15:00 hs and collector tilt angle 44 °.

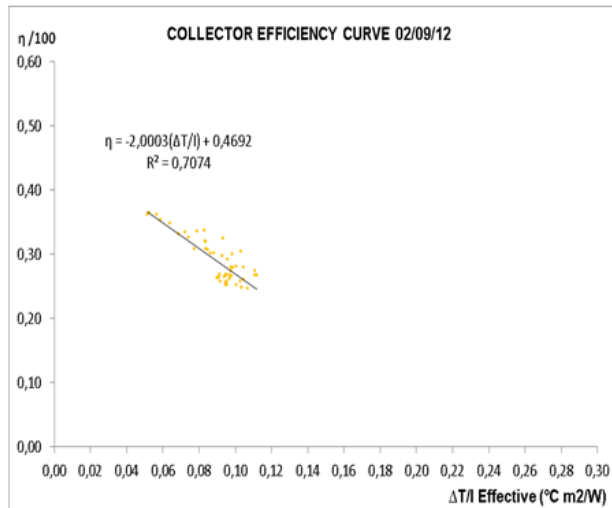


Figure 16. Efficiency collector as a function of ΔT/I the day 02/09/12, and flow velocity 1.7 m/sec

Green points: in the schedule from 13:00 hs to 14:00 hs and collector tilt angle 44 °.

Yellow points: in the schedule from 14:00 hs to 15:00 hs and collector tilt angle 44 °.

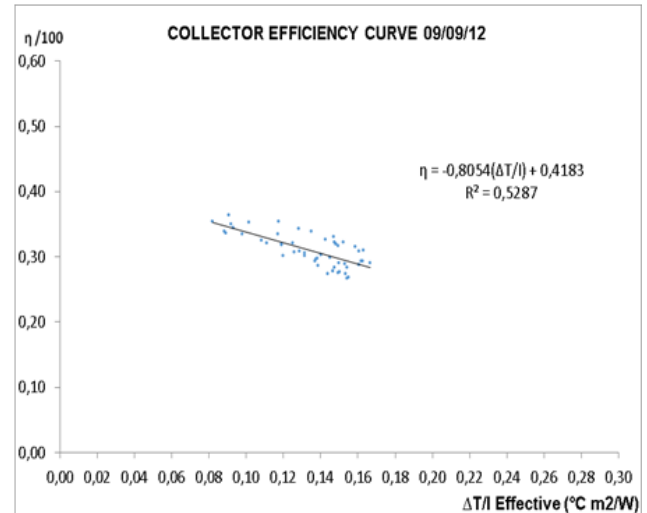


Figure 19. Efficiency collector as a function of ΔT/I the day 09/09/12, and flow velocity 1.35 m/sec

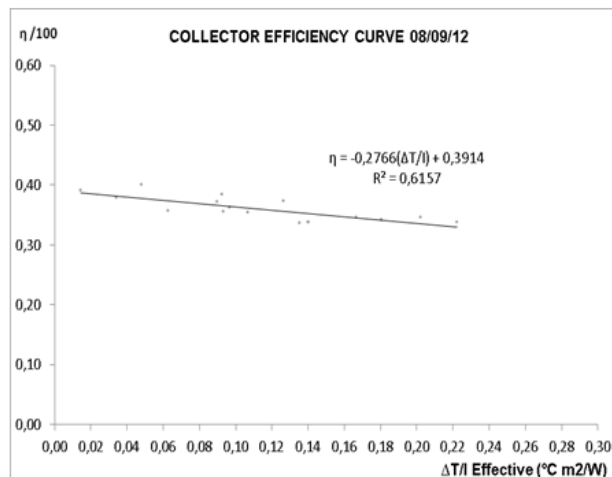


Figure 17. Efficiency collector as a function of ΔT/I the day 08/09/12, and flow velocity 1.43 m/sec

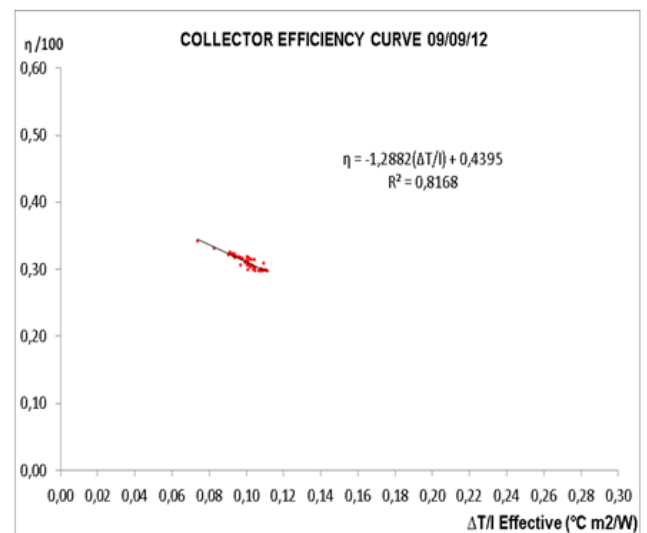


Figure 20. Efficiency collector as a function of ΔT/I the day 09/09/12, and flow velocity 1.5 m/sec

Blue points: in the schedule from 11:00 hs to 12:00 hs and collector tilt angle 40 °.

Red points: in the schedule from 12:00 hs to 13:00 hs and collector tilt angle 40°.

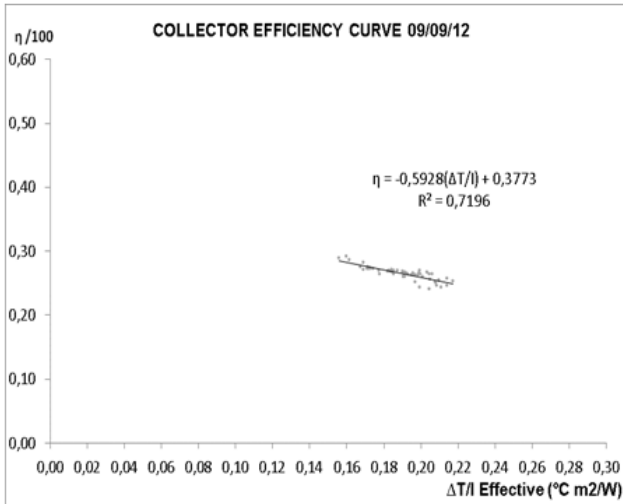


Figure 21. Efficiency collector as a function of $\Delta T/I$ the day 09/09/12, and flow velocity 1.15 m/sec

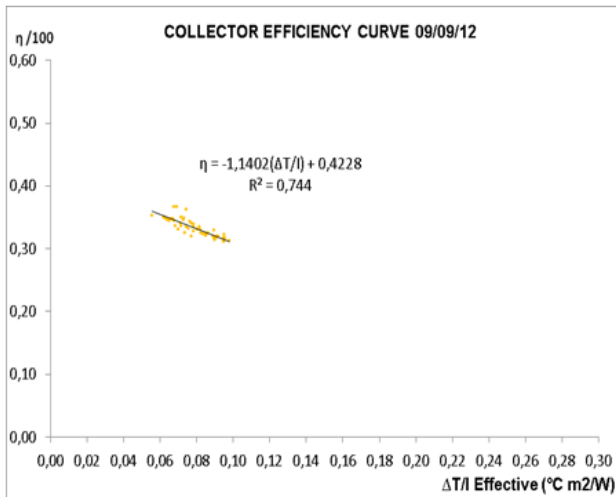


Figure 22. Efficiency collector as a function of $\Delta T/I$ the day 09/09/12, and flow velocity 1.58 m/sec

Green points: in the schedule from 13:00 hs to 14:00 hs and collector tilt angle 44°.

Yellow points: in the schedule from 14:00 hs to 15:00 hs and collector tilt angle 44°.

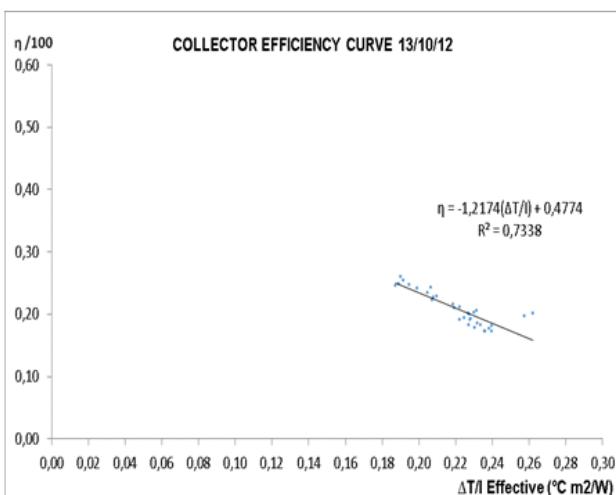


Figure 23. Efficiency collector as a function of $\Delta T/I$ the day 13/10/12, and flow velocity 1.1 m/sec

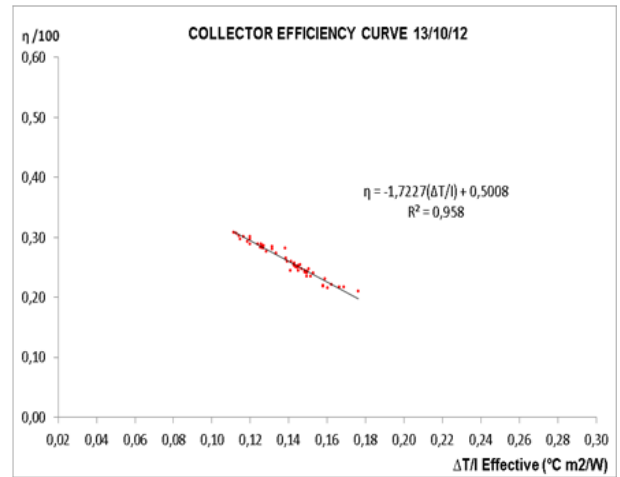


Figure 24. Efficiency collector as a function of $\Delta T/I$ the day 13/10/12, and flow velocity 1.75 m/sec

Blue points: in the schedule from 11:00 hs to 12:00 hs and collector tilt angle 40°.

Red points: in the schedule from 12:00 hs to 13:00 hs and collector tilt angle 40°.

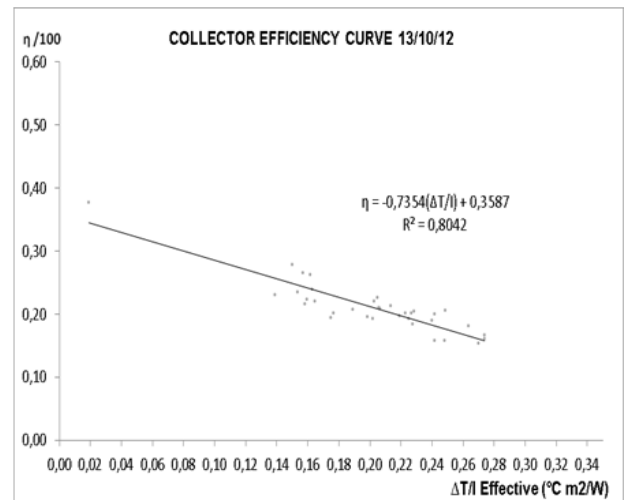


Figure 25. Efficiency collector as a function of $\Delta T/I$ the day 13/10/12, and flow velocity 1.15 m/sec

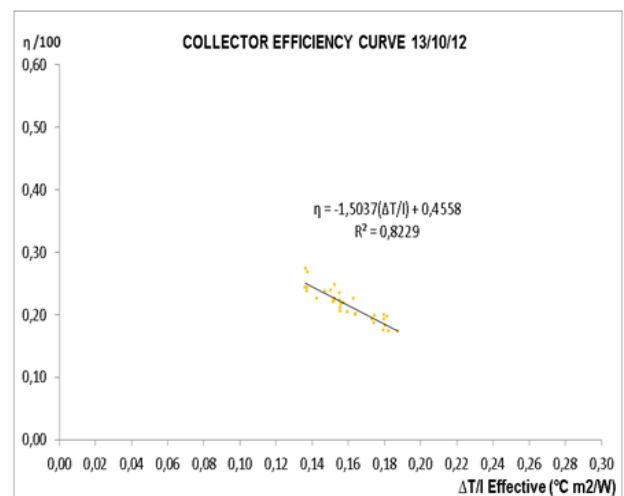


Figure 26. Efficiency collector as a function of $\Delta T/I$ the day 13/10/12, and flow velocity 1.7 m/sec

Green points: in the schedule from 13:00 hs to 14:00 hs and collector tilt angle 44°.

Yellow points: in the schedule from 14:00 hs to 15:00 hs and collector tilt angle 44°.

From the graphs (1-26), can be displayed, that practically does not have much incidence changing device tilt angle of 40 ° to 44 ° and vice versa, during the days tested.

For the date 14/07/12, in Figure 1, two graphs are observed, in order to visualize two curves at different times (11:20 am - 12:00 pm and 13:00 pm - 14:00 pm) and the same flow velocity (1.25 m/sec.), is determined a higher performance from 13:00 pm to 14:00 pm, mainly due to increased solar irradiance available. The same happens in figure 2, it has 2 curves at different times (12:00 pm - 13:00 pm and 14:00 pm - 15:00 pm), with flow velocity of 1.8 m/sec. The highest performance was presented in the time zone from 12:00 pm to 13:00 pm, given the same consideration of the above.

Both Figure 1 and Figure 2, is established a higher flow velocity, improves performance of the device [11].

For the date 20/07/12, are presented Figure 3 and Figure 4, observed higher performance for graphic higher flow velocity. The same happened on 08/09/12.

For the date 25/08/12, worth the same considerations as for the date 20/07/12.

Another detail that can be visualize, is that at equal performance, the schedules that showed higher flow velocities have values lower abscissa, improving its operation respect to the lower flow velocity. The latter can also be seen in the dates 02/09/12, 09/09/12 and 13/10/12.

For the date 26/08/13 you can not visualize what said so far, as there were partial cloudiness, affecting performance.

The performance curves of 11/09/12 were not presented, as it has no representativeness for this analysis, by out of service the fan. In most graphs, the correlations are acceptably adjusted to the model, because R^2 is quite high.

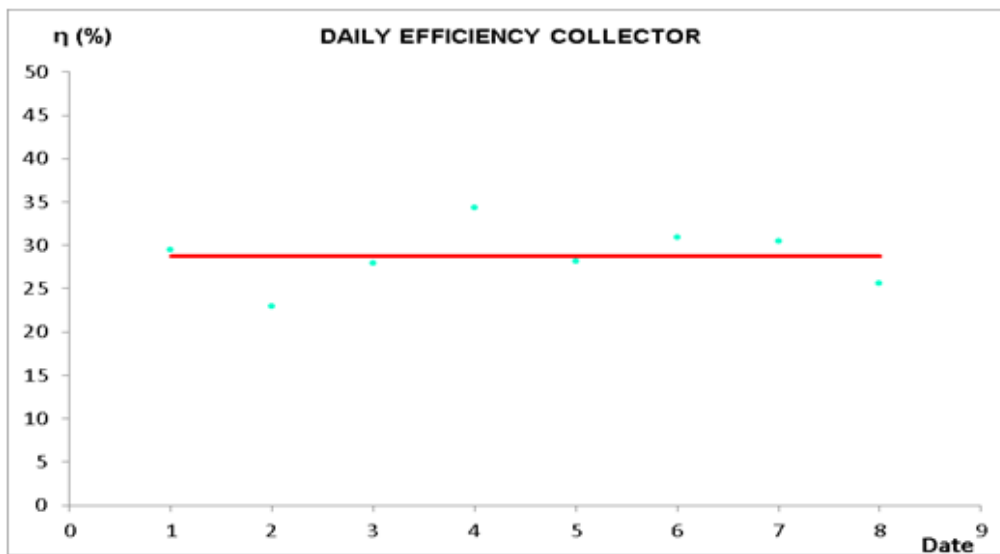


Figure 27. Average Daily Efficiency of solar air collector, along with the trend line

To determine Figure 27, daily instantaneous values of efficiency are averaged. The red line represents the average efficiency during the period considered and is equal to 28.72%. The calculations were averaged daily time of experience.

On the horizontal axis of this graph, there are numbers that describe the experience dates. So, 1 equivalent to 14/07/12; 2 equivalent to 1 20/07/12; 3 equivalent to 25/08/12; 4 equivalent to 26/08/12; equivalent to 02/09/12; 6 equivalent to 08/09/12; 7 equivalent to 09/09/12; and 8 equivalent to 13/10/12.

The Figure 27 shows that the overall daily efficiencies of collector, are below 35%. This occurred because for the calculation has taken an average efficiency between the two compartments; and given the collector geometry, it is known that at the upper, the efficiency is higher than in the lower part. On the other hand, it may have been heat leaks not considered by the unions of polycarbonate, in some moments of experimentation.

This type of collectors, where air circulation is achieved both above and below the absorber plate, has greater efficiencies (equal size to the absorber), because the fluid has more contact area, equality to mass flow, with respect to the collectors where the fluid flows on one face of the absorber.

9. Cost of Solar Collector

The total cost of the device is equivalent to u\$S 863.87, of estimated manner, and does not consider the cost of the fan nor the measuring elements, and are found discriminated in percentages of the total value as shown in Table 6:

Table 6. Components of the solar collector and prices

| COST OF COLLECTOR (u\$S) | | PERCENTAGE OF COST (%) |
|----------------------------------|--------|------------------------|
| Galvanized Plate | 78,02 | 9,03 |
| Polycarbonate cover | 69,63 | 8,06 |
| Fiber glass cover | 136,61 | 15,81 |
| Expanded Polyethylene Insulating | 33,22 | 3,85 |
| Plastic 200 micron | 3,02 | 0,35 |
| Aluminum Profiles | 41,95 | 4,86 |
| Iron straps | 6,21 | 0,72 |
| Polycarbonate Union | 18,46 | 2,14 |
| Regulating air and Hood | 125,84 | 14,57 |
| Aluminium tape and Fiselina | 2,92 | 0,34 |
| Neutral sealant | 5,80 | 0,67 |
| Insulating Gum | 6,71 | 0,78 |
| Screws | 11,74 | 1,36 |
| Black matte paint | 8,39 | 0,97 |
| Structural Pipe Supports | 25,17 | 2,91 |
| Hinges | 56,63 | 6,56 |
| Several | 33,56 | 3,88 |
| Labor to build the collector | 200,00 | 23,15 |
| TOTAL | 863,87 | |

It is observed that the determining cost is labor for constructing the device. It can be seen that the higher cost material relative is cover fiberglass. However this material could be replaced by other materials such as polycarbonate, which has a lower price.

10. Conclusions

The yields of the device are around between 20% and 35%, considering an energy consumption of the fan; added to this, its relatively low cost, makes the device competitive as air heat exchanger compared to other models of solar air collectors.

From a construction point of view, the lack of trade measures polycarbonate sheets, requires cutting and connecting them according to the length of the device, with the possible loss of efficiency in the unions with the passage of time. It is therefore not advisable to build this type of collectors in more than 2.1 m long. Taking into account the considerations developed flow, and under this trade restriction, It would be convenient to work with smaller equivalent diameter, to achieve have developed flow to shorter lengths collector.

For the construction of this collector, requires paying much attention to rigid polycarbonate sheets and fiberglass, as well as the same structure of the device. If the stiffness is not good, may fall down the/s plate s upper/s; and even fall down below by varying the inclination angle of the collector.

Nomenclature

| | |
|----------------------------------|--|
| qu | Useful energy collector (kW), |
| η planta energía térmica | Performance of a thermal power plant, |
| η transmisión energía elect | Performance transmission of electric power, |
| η motor ventilador | Performance of the fan motor used, |
| η ventilador | Fan performance, |
| r | Radius minor of an ellipse (m), |
| s | Radius larger of an ellipse (m), |
| De | Equivalent diameter (m), |
| P | Perimeter of an ellipse (m), |
| 0.18 | Factor conversion of mechanical energy into thermal energy in our country, |
| I | Intensity of Radiation on Inclined surface (Wh/m^2), |
| Cp | Specific Heat of Humid Air ($\text{kJ/kg}^\circ\text{C}$), |

| | |
|----------------------|---|
| Tp | Average temperature of absorber plate ($^\circ\text{C}$), |
| m | Air mass (kg), |
| A | Catchment surface area (m^2), |
| A1 | Ellipse Area (m^2), |
| Af | Flow Area (m^2), |
| ρ | Humid Air Density (Kg/m^3), |
| v | Air velocity inside the collector (m/seg.), |
| Up | Global heat transfer coefficient ($\text{kW/m}^2\text{aC}$), |
| Ta | Ambient temperature or input to the collector ($^\circ\text{C}$), |
| Tms | Average temperature of fluid outlet ($^\circ\text{C}$), |
| P | Pumping power air by the fan (kW), |
| α_p, α_c | Absorbance absorber plate and polycarbonate cover, |
| ξ_p, ξ_c | Emissivity absorber plate and polycarbonate cover, |
| ρ_p, ρ_c | Reflectance absorber plate and polycarbonate cover. |

References

- [1] Meinel A. B., Meinel M. P. (1982): Aplicaciones de la Energía Solar Térmica, Reverté, España, pp: 464-465.
- [2] Espinoza R. et al., 2010. Secado Solar de Productos Agroalimentarios en Iberoamérica, Espinosa, Saravia. 1° ed. Salta, pp: 122-131.
- [3] Duffie J., Beckman W., 1980. Solar Engineering of Thermal Processes, John Wiley & Sons, E.E.U.U., pp: 257, 267, 297-299, 689, 698-702.
- [4] Ibáñez Plana M., Rosell Polo J., Rosell Urrutia J., 2005. Tecnología Solar, Mundi-Prensa, España, pp: 233-24.
- [5] Perelló Daniel A., 2008. Policarbonato versus vidrios en Colectores Solares, Universidad Nacional de Salta, Salta, pp: 2-6, 9-11, 27-31.
- [6] Incropera F., DeWitt D., 1999. Fundamentos de Transferencia de Calor, 4° ed, Prentice Hall, México, pp: 420-421, 425-426, 482, 487, 490-491, 506, 509, 515, 289-290.
- [7] American Society of Heating Refrigerating and Air-Conditioning Engineers Inc. (1977). *Ashrae Handbook & Product Directory*. New York: Author.
- [8] Felipe Blanch J. J., López Martínez J. A., 1999. Sistemas Solares Térmicos de Baja Temperatura, Universidad Politécnica de Cataluña, Barcelona, pp: 20.
- [9] Bistoni, S. et al., 2003. Análisis Teórico de un Colector Solar de Aire, ASADES, Vol. 7, Argentina.
- [10] Apurba L., 2010. Optimal thermo-hydraulic performance of solar air heater having chamfered rib-groove roughness on absorber plate. *International Journal of Energy and Environment*, 1, 687-688.
- [11] Hernández A. et al. (2007). Diseño, Construcción y Primeros Ensayos de un Colector Solar Calentador de Aire de tipo Loop Convectivo para Calentamiento de Edificios, ASADES, Volumen 11, Argentina.